Experiments in Fluids 11, 268–278 (1991)

Experiments in Fluids

Experiments characterizing the interaction between two sprays of electrically charged liquid droplets

S. R. Snarski and P. F. Dunn

Department of Aerospace and Mechanical Engineering, University of Notre Dame, Notre Dame, IN 46556, USA

Abstract. Experiments were conducted to characterize the interaction between two sprays of electrically charged ethanol droplets. The micrometer-size droplet sprays were generated electrohydrodynamically by applying a high positive voltage to two adjacent parallel needles that were located above a distant, electrically grounded funnel. The resultant droplet axial and lateral velocity components and diameter were measured as a function of needle spacing and applied voltage using a Phase Doppler Particle Analyzer. Data were acquired at two axial positions below the needles' tips, for two needle spacings, four applied voltages and at a single flow rate.

The results revealed that an increase in applied voltage yielded an increase in the spray charge density. This produced an increase in both the axial and lateral droplet velocity components and a decrease in the droplet Sauter mean diameter and in its variation across the spray. An increase in needle spacing yielded a decrease in the axial velocity component. The lateral velocity component and the Sauter mean diameter, however, were not noticeably affected by this increase. Photographic data established a relationship between the lateral half-width of the spray and axial distance. This was used to identify a nondimensional similarity between the axial mean velocity component and lateral position. The results collectively support that appropriate variations in the applied voltage and needle spacing can yield more spatially uniform mean velocity component and Sauter mean diameter profiles. These variations bring about increased mixing between the two needles' sprays and, thus, an enhanced development of the combined droplet spray.

1 Introduction

This paper presents the results of experiments conducted to characterize the interaction that occurs between the charged droplets of two electrohydrodynamic (EHD) sprays. This method of droplet generation already has been exploited to yield several practical applications, including ink jet printers, crop and dust sprayers, electrostatic paint sprayers and colloid thrusters. Its technology is supported primarily by a number of basic research studies that were conducted during the 1960s and 1970s (e.g., Hendricks 1962, Hogan and Hendricks 1965, Pfeifer and Hendricks 1967, Bailey 1974, Jones and Thong 1971, Kelly 1976, 1978 and Ogata et al. 1978) that elucidated the specific mechanisms of droplet generation and the relationships between droplet size and charge and system operating parameters [1].

With the recent development of advanced in situ laser diagnostic systems, it is now possible to obtain more accurate and spatially specific information on the velocity and/or diameter of droplets within EHD sprays. Such detail was not possible in earlier studies. This paper reports the first laser diagnostic measurements of the velocity components and diameters of droplets within two EHD sprays generated from parallel needles. In addition, the present work also determines the effects of applied voltage, therefore spray charge density, and needle spacing on the resultant mean droplet sizes and velocity components, and identifies similarity in the spatial development of such sprays.

2 Initial considerations

The dynamics of droplet motion within an EHD spray is admittedly complex and, at present, difficult to completely analyze. Some insight, however, into the physics of this problem can be gained by estimating the magnitudes of the external forces acting on an individual droplet within various regions of the spray. This can be done by examining the governing equation of motion for the droplet.

The generalized force balance equation for a spherical droplet in motion (Hidy 1984) first can be simplified somewhat for the problem under consideration by neglecting two forces; the force required to accelerate the apparent mass of the droplet relative to the ambient gas and the drag force associated with unsteady motion (the Basset term). This can be done in the present situation because the gas density is negligible as compared to the droplet density. The force balance on a droplet of spherical diameter, d_d, mass, m_d, and charge, q_d, in motion in the presence of other droplets of similar electric charge and externally imposed electric and gravitational fields then can be written as:

$$m_d \frac{d\hat{V}_d}{dt} = \hat{F}_G + \hat{F}_D + \hat{F}_E$$

[1] See Snarski (1988) for a recent review

where the gravitational, aerodynamic drag and electric forces for this system are:

$$\hat{F}_G = m_d\, g\hat{z}\,,$$

$$\hat{F}_D = \frac{-C_D\,\pi\,\varrho_m\,d_d^2}{8}\sqrt{(V_{x_d}^2 - V_{x_m}^2)+(V_{z_d}^2 - V_{z_m}^2)}\,[\hat{V}_d - \hat{V}_m]$$

and

$$\hat{F}_E = q_d\,\hat{E}\,,$$

in which $\hat{V}_d$ denotes the droplet velocity, $\hat{V}_m$ the medium (air) velocity, C_D the drag coefficient, $\hat{E}$ the electric field, ϱ_m the medium density, g gravitational acceleration, ε_0 the permittivity of free space (8.85 E − 12 F/m), which closely approximates that in air, and x and z the lateral (horizontal) and axial (vertical) coordinates, respectively. The droplet drag coefficient, C_D, is a function of the Reynolds number, Re, which equals $\varrho_m\, d_d\sqrt{(V_{x_d}^2 - V_{x_m}^2)+(V_{z_d}^2 - V_{z_m}^2)}/\mu_m$. The expression for the drag coefficient used herein is $C_D = 24\,[1 + 0.15\,Re^{0.687}]/Re$. This was developed by Schiller and Naumann for $1 \le Re < 800$ (Clift et al. 1978) and is an empirical formula that most closely matches measured values for the Reynolds number range of the present experiment ($0.1 < R < 40$).

The simplified equation of motion for the droplet can be written nondimensionally as:

$$\frac{d\hat{V}_d^*}{dt^*} = \frac{\hat{z}^*}{Fr} - \frac{C_D\,Re}{24\,Stk}(\hat{V}_d^* - \hat{V}_m^*) + (Ne^2)\,(\hat{x}^* + \hat{z}^*)$$

in which the additional nondimensional terms, the Stokes, Froude and electric numbers, are defined as $Stk = d_d^2\,\varrho_d\,V_d/18\,\mu_m\,D$, $Fr = V_d^2/g\,D$, and $Ne^2 = F_E\,D/m_d\,V_d^2$, respectively. Here, the velocity and coordinate vectors are nondimensionalized with respect to D and τ, which represent the characteristic distance and time of this system, and μ_m is the absolute viscosity of the medium.

The electric force on the droplet, $\hat{F}_E$, results from two contributions; one from the externally imposed electric field produced by the potential established between the needle and a distant, electrically-grounded plane, $\hat{F}_{E_1}$, and the other by the Coulombic repulsion of the neighboring droplets of similar electric charge, $\hat{F}_{E_2}$.

$\hat{F}_{E_1}$ has lateral and axial components. These can be approximated closely by those derived by Jones and Thong (1971) for an electric field between an isolated finite line of charge (a needle) and an infinite, grounded electrode. The magnitude of $\hat{F}_{E_1}$ can be determined directly by substituting the coordinates of the position of interest into its component expressions.

$\hat{F}_{E_2}$ also has lateral and axial components. The range of the magnitude of the $\hat{F}_{E_2}$ force can be estimated by determining that on a droplet at the center of the spray and at its periphery. At and near the center, this force is relatively small because the droplet is surrounded essentially by an equal number of droplets in all directions. At the periphery, this force is the summation of the repulsive forces from all the droplets within the spray, which is equivalent to a repulsive force from a neighboring "cloud" of droplets. The magnitude of this force has been estimated by Bailey (1988) to be:

$$F_{E_2} = (n\,R_c/3\,\varepsilon_0)\,q_d^2$$

in which n is the number concentration of droplets in the cloud and R_c the cloud radius. This can be written in a more general sense by introducing the variable k_e, where:

$$k_e = 4\,\pi\,n\,R_c\,s^2/3$$

in which s is the spacing between the droplet and cloud center. The magnitude of the force then becomes:

$$F_{E_2} = (k_e/4\,\pi\,\varepsilon_0)\,q_d^2/s^2$$

In the limit, as $R_c \to s$ and $n\,V_c \to 1$, $k_e \to 1$ and this expression reduces to that for the simple electrostatic repulsive force between two droplets of the same diameter.

Using these expressions, the magnitude of the forces identified in the equation of motion can be estimated within various regions of the spray. For this study, these magnitudes were estimated in three regions; one in which the axial coordinate distance was of the order of the needle's external radius, one of the order of its length (which is the region in which the subject data was taken), and the other of the order of the distance between the needle and the grounded plane. In the later two, the force magnitudes were estimated both at the center and the periphery of the spray. The axial and lateral coordinates of these locations are given in Table 1.

Table 1. Force magnitude estimates for various positions within the spray

Position no.	x (cm)	z (cm)	F_{E_1} − 15 kV (N)	F_{E_2} − 15 kV (N)	F_{E_1} − 30 kV (N)	F_{E_2} − 30 kV (N)
1	0.020	0.020	7.39 E-6	8.53 E-10	1.48 E-5	5.68 E-9
2	1.500	1.500	9.79 E-8	6.30 E-8	1.96 E-7	4.20 E-7
3	0.020	1.500	4.75 E-6	8.53 E-10	9.50 E-6	5.68 E-9
4	3.000	3.000	4.81 E-8	1.26 E-7	9.62 E-8	8.40 E-7
5	0.020	3.000	4.55 E-6	8.53 E-10	9.11 E-6	5.68 E-9
6	38.00	37.98	3.83 E-9	1.60 E-6	7.66 E-9	1.06 E-5
7	0.020	37.98	6.04 E-9	8.53 E-10	1.21 E-8	5.68 E-9

Note: F_G (N) = 3.24 E-11; F_D − 15 kV (N) = 1.42 E-8; F_D − 30 kV (N) = 2.85 E-8

The values of the magnitudes of the gravitational, drag and two electric forces are listed in Table 1 for the lowest and highest applied potentials investigated (15 and 30 kV). The droplet diameter was assumed to be 20 μm and velocity the average of those measured at that applied voltage (3.0 m/s and 5.3 m/s for the 15 kV and 30 kV cases, respectively).

These and other estimates made over the range of diameters that are typical of such EHD sprays (1 μm $< d_p <$ 200 μm) revealed that in all regions the gravitational force on a droplet was negligible, i.e., at least two orders of magnitude less than the other forces. Further, the magnitude of the composite electric force, F_E, was always at least one order of magnitude greater than the drag force, except in the region at the center of the spray very near the ground plane (position no. 7). In these estimates, the drag force was conservatively overestimated by assuming that it was based upon the droplet velocity only and not upon the relative velocity between the droplet and the air. Further, the droplets were assumed to be charged to their maximum (Rayleigh) limit. Near the periphery of the spray (positions 2, 4 and 6), the F_{E_1} term dominates in its contribution to the electric force, whereas near the center of the spray (position 1, 3 and 5) the F_{E_2} term does. It is interesting to note that at position 1, which is very near the needle's tip, the magnitude of the F_{E_2} force for large droplets (when d_p is of the order of 1,000 μm) becomes comparable in magnitude to that estimated by Bailey (1988) for a charged pendant droplet as it departs from the tip of a charged needle.

These results imply that over the scale lengths of the subject experiment, when conducting droplets are charged to within an order of magnitude of their Rayleigh limit, that the electric forces predominantly govern the droplet dynamics of the spray and not the gravitational and drag forces. This is the case for the subject experiments.

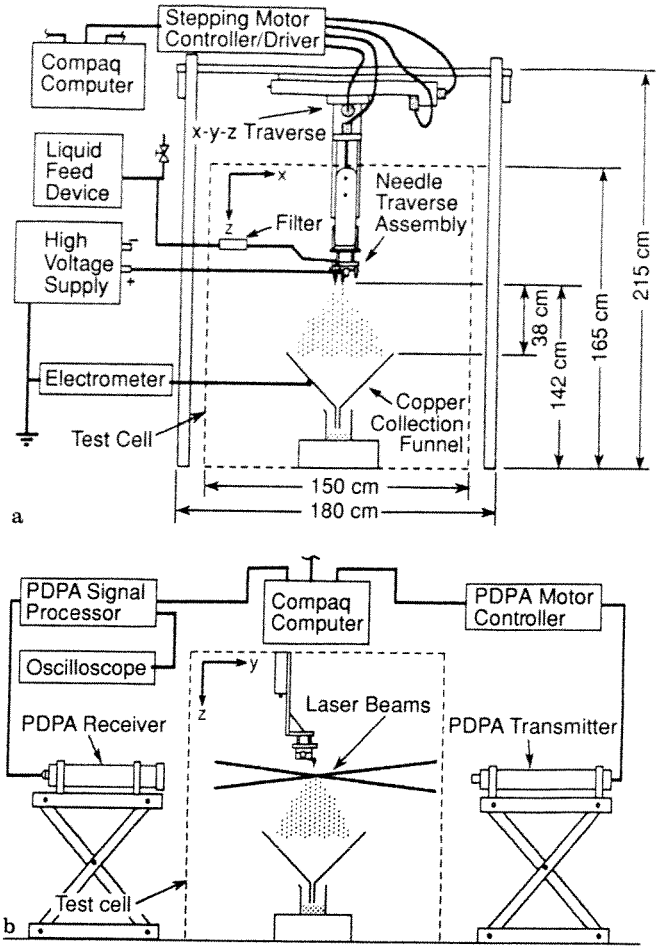

Fig. 1 a and b. Schematic of the experimental apparati; **a** front view; **b** side view

3 Experimental apparatus and procedure

In the present experiments, liquid ethanol droplet sprays were generated by establishing a high, positive electric potential between the tips of two electrically conducting needles and a distant, electrically grounded funnel. A schematic of the experimental apparati is shown in Fig. 1 a and b. The main components of the system included a fluid delivery system, an electrical charging system, a needle positioning and traversing apparatus and a particle analyzer, laser diagnostic system.

The fluid delivery system consisted primarily of a liquid reservoir and feed device, flexible Tygon™ tubing, a two-needle discharge apparatus and a liquid collection device. Liquid droplets that sustained a fixed dripping rate ($\sim$0.5 to 1 Hz) in the absence of an applied voltage were generated by pumping the liquid through the system using a 50 ml syringe mounted on a Harvard, Model No. 906, variable speed-constant volumetric flow rate, infusion-withdrawal pump. A flow rate of 0.79 ml/min (4.5 mg/s ethanol per needle) was chosen for these experiments. The liquid then passed through several lengths of 1/4 in. (0.635 cm) I.D. Tygon™ tubing, a 1/4 in. (0.635 cm) Whitey valve, an in-line 2 μm Nupro Series 8H filter and a stainless steel manifold that divided the liquid into two paths. Once divided, the liquid passed through two perfectum® 27 gauge blunt tip stainless steel hypodermic needles (216 μm I.D., 406 μm O.D., 1.91 cm length). From the two needles, the liquid discharged into a 61 cm diameter copper funnel mounted on a 1,000 ml beaker placed at approximately 38 cm below the needles' tips.

A Glassman High Voltage 3 kW, 0–50 kV DC power supplied a high D.C. voltage of positive polarity with respect to the collection funnel to the needles. Experiments were conducted at applied, positive potentials of 15, 20, 25 and 30 kV. Measurements of the droplet current were performed by monitoring the current to ground through a Keithley Model 617 Programmable Electrometer. An average droplet current was determined at each applied voltage during a separate experiment in which a spray was generated from on needle only at a mass flow rate of 4.5 mg/s.

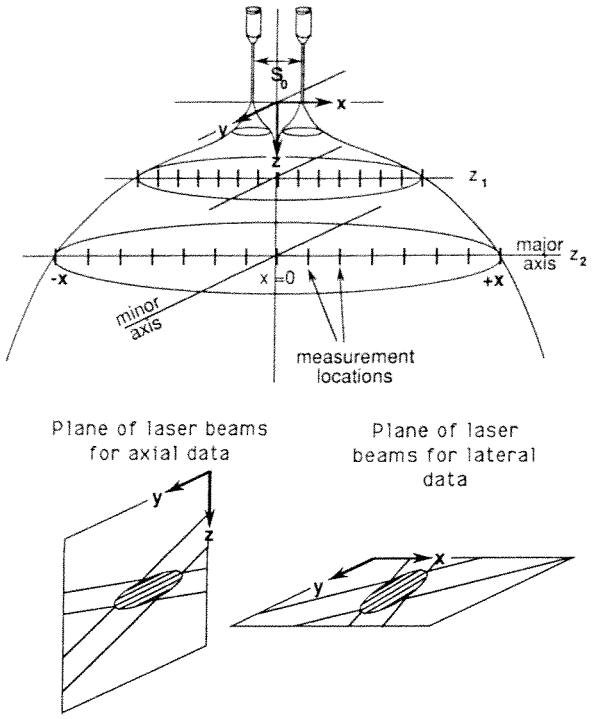

Fig. 2. EHD spray coordinate system

A needle positioning and traverse assembly, which also housed the flow separating manifold and high voltage connections, was used to vary the separation distance between the two needles. This assembly was constructed of aluminum and Delrin and supported a 1 cm diameter stainless steel screw which traversed an aluminum slider that was connected to one of the needles.

The axial and lateral droplet velocity components and diameters of the interacting sprays were measured using a Phase Doppler Particle Analyzer (PDPA), as described by Bachalo and Houser (1984), containing a Spectra Physics Model SP-106 10 mW Polarized He-Ne laser. The system's Compaq computer also was interfaced with a Velmex 8300 series stepping motor controller/driver. This moved the entire needle assembly such that the fixed PDPA transmitter and receiver could probe the entire flow field beneath the two needles. In the present experiments, the PDPA was configured to receive the scattered light in the 30° off-axis forward scattering mode. The orientation of the laser beams and probe volume relative to the two needles and combined spray for both the axial and lateral data is presented in Fig. 2. Because only two needles were used, the combined spray inherently was not axisymmetric. Consequently, the results obtained in these experiments represent only what was occurring along the major axis of the spray, as denoted in the figure.

The camera system used for the photography of the droplet sprays consisted of an Olympus OM-1 camera body with a Recordata Back 4, Motor-Winder 2 and Kodak Tmax, 400 ASA black and white film. The lens system included an Olympus Telescopic Auto Extension Tube 65-116 mm and an Olympus Zuiko Macro 135 mm F4.5 lens. This system was chosen because of it produced high magnification (3.5 to 7×) at relatively large focal lengths (up to ~2 m).

Both continuous and stroboscopic lighting techniques were utilized to determine the boundaries of the sprays and the local droplet structure therein during separate experiments. This was accomplished by photographing the sprays in front of a flat black back drop and by back lighting the field with two high intensity lamps, both at an angle of approximately 30° with the camera-flow field centerline. The two lamps were placed at a distance of approximately 3 m from the flow field at the same elevation as the needles. A Colortran, model B10064 lamp with a GE 600 W bulb was used for one source while a Lowel Tota-Lamp with a Sylvania 750 W Tungsten Halogen, 3,200 K color temperature bulb was used for the other. Aperture and shutter speeds of f/16 and 4 s, f/11 and 2 s and f/8 and 1 s were used, depending upon the particular flow characteristics. The stroboscopic photographs were taken with the same configuration except the two incandescent lamps were replaced with a Strobolume strobe system. This consisted of a GenRad 1540 Strobolume power unit, 1540-P2 Strobolume lamp (10 μs flash at 0.25 Ws and 0.5×10^6 cd) and a 1540-P3 Strobolume Control Unit. The strobe lamp was positioned behind the flow field to provide back lighting (forward scattering), which provided the best illumination of the droplets.

Mean velocity and Sauter mean diameter profiles across the lateral span of the interacting droplet sprays at a given axial position were constructed using the mean values computed from 10,000 valid signals obtained at each of the 15 lateral positions between the "edges" of the sprays. An "edge" was defined as that lateral position beyond which 10,000 validations could not be achieved within 300 s. These mean values represent at each position a spatial rather than temporal average because they were obtained over a time period ranging from approximately 10 to 120 s. A total of 480 raw data sets were obtained in these experiments. For brevity, only the mean quantities obtained at all of the positions are presented herein. Some velocity component and diameter distributions at various locations are given in the subsequent section. More detailed information is provided in the thesis of Snarski (1988).

Droplet average specific charges were also computed using the average droplet current data and the measured droplet average mass mean diameters. All of the resultant droplet average specific charges, which were in the range from 0.1 to 1.0 C/kg, were found to be within an order of magnitude of their Rayleigh limit. This compares well in the subject droplet diameter range with the results of other investigators using similar systems and different, conducting liquids (Hendricks 1962, Krohn 1974, and Lue and Kelly 1987).

The average droplet current and mass flow rate data were also used to determine the average charge density level of the sprays. This has been shown by Kelly (1984) to be the essential correlating parameter for EHD sprays. The resultant

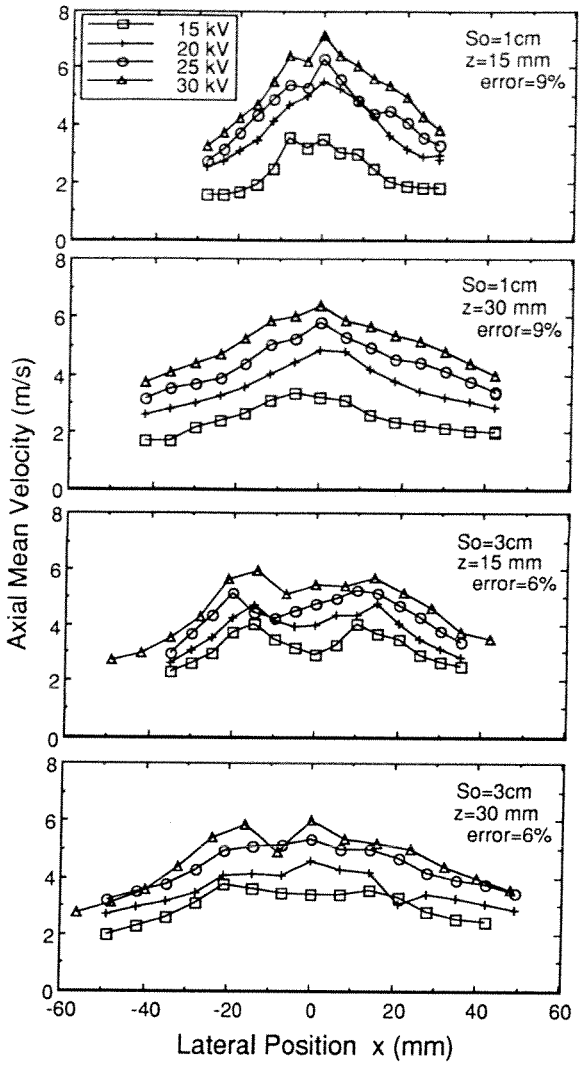

Fig. 3. Droplet axial mean velocity profiles for 1 and 3 cm needle spacings and 15 and 30 mm axial distances

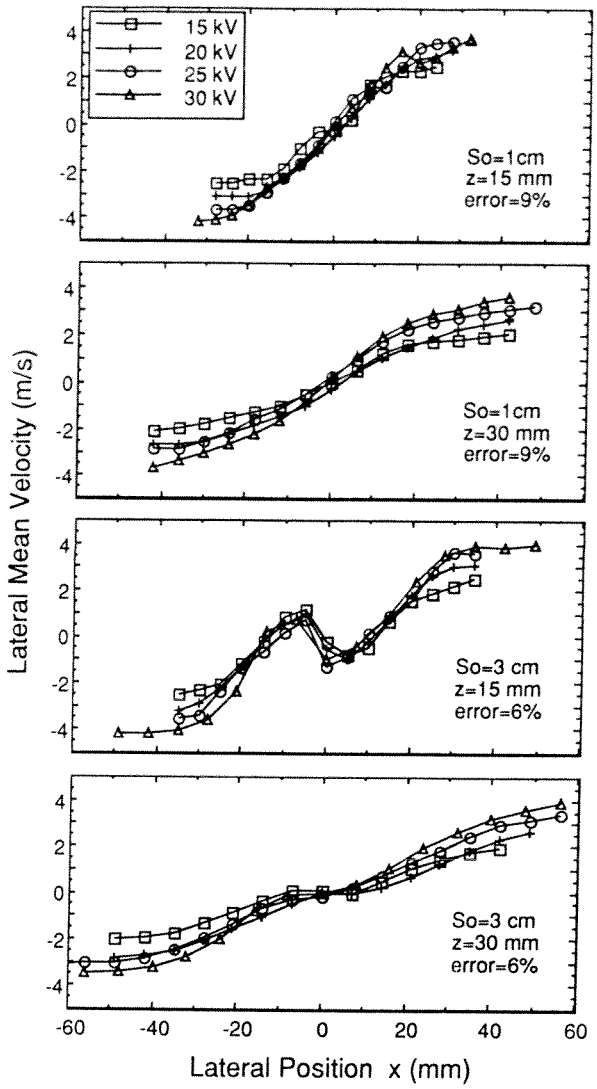

Fig. 4. Droplet lateral mean velocity profiles for 1 and 3 cm needle spacings and 15 and 30 mm axial distances

average charge density levels for the applied voltages of 15, 20, 25 and 30 kV in the present experiment were determined to be 59, 116, 184 and 278 C/cm^3, respectively.

Estimated uncertainties in the measured quantities were from 1 to 2% for the volumetric flow rate, with a 2.1% maximum flow rate discrepancy between the two needles, less than 1% for the measured voltage and ± 0.5 mm for the needle spacings (5 or 1.7% uncertainty for the 1 and 3 cm spacings, respectively). The uncertainty for the probe volume location was also less than 1%, while the uncertainty in the measured velocity was assumed to be 1%, as estimated by Bachalo and Houser (1984). The typical uncertainty in the measured diameter was 4%. The overall range of uncertainty in the measured diameter for the actual diameters measured in the present experiments was from 2 to 16%, based upon the recent PDPA droplet sizing calibration studies of O'Hern et al. (1989). The uncertainty in the current measurements was from 1% at the lowest voltage, where all the spray was collected by the funnel, to approximately 30% at the highest voltage, where the spray width exceeded that of the funnel. The uncertainty in the measurement of the spray widths from the photographs was 1%.

4 Results and discussion

4.1 Droplet mean velocity components

The axial and lateral mean droplet velocity component profiles across the lateral span of the interacting sprays for both needle spacings and axial locations are presented in Figs. 3 and 4. Each of the velocity components shown is the mean value of the velocity component distribution at that measurement point. The total experimental error for the mean velocity component that resulted from uncertainties in the PDPA velocity component measurement, mass flow rate,

probe volume position and needle separation distance was 9% and 6% for the 1 cm and 3 cm needle spacings, respectively.

The axial mean velocity component profiles for the 1 cm needle spacing shown in Fig. 3 are characterized by a mean velocity component magnitude that is maximum at the center and decreasing in the lateral direction. The lateral mean velocity component profiles, shown in Fig. 4, have a mean velocity component magnitude that is zero at the center and increasing in the lateral direction. In this figure, lateral velocity components to the left of the centerline are displayed as negative in value because they are opposite in direction to those on the right of the centerline. For both the axial and lateral mean velocity component cases, the magnitudes of the velocity components asymptotically approach constant values at the lateral edge of the sprays for each applied voltage.

The axial mean velocity component profiles for the 3 cm needle spacing and 15 mm axial location shown in Fig. 3 are characterized by two local maxima, where the two lateral positions at which the mean velocity component magnitude is maximum are those of the two needles' centerline axes. In addition, the magnitudes of these two maxima decrease as the axial location is increased. This does not occur with the 1 cm needle separation because the axial range in which data was taken was sufficiently far away from the needles such that the velocity component profiles from the two needles apparently had already merged.

The lateral mean velocity component profile at the 15 mm axial location shown in Fig. 4 has a mean velocity component magnitude that is zero at the center. In the lateral direction, this velocity component decreases, then increases, returning to a magnitude of approximately zero at the lateral positions of the two needles' centerline axes. This is the direct result of the inward lateral migration of the droplets of the two sprays between the two needles' axial centerlines. With a further increase in the lateral direction, the lateral mean velocity components increase and asymptotically approach a final value. At the 30 mm axial location, the lateral mean velocity component magnitude is approximately zero over a small center region and then increasing in the lateral direction.

These aforementioned axial and lateral mean velocity component profile results are summarized in the qualitative illustrations of Figs. 5a and b. As shown in Fig. 5a which illustrates the axial mean velocity component profile results, for the 1 cm spacing at the first axial position, the two separate sprays have already merged and begun to develop into a single, uniform spray. At the second axial location, the spray has already become more spatially uniform. For the 3 cm spacing case, on the other hand, the two separate sprays have just begun to merge at the second axial position, while at the first, they are still somewhat distinct individual sprays. These interpretations are supported further by the lateral mean velocity component profile results shown qualitatively in Fig. 5b. These results collectively illustrate that

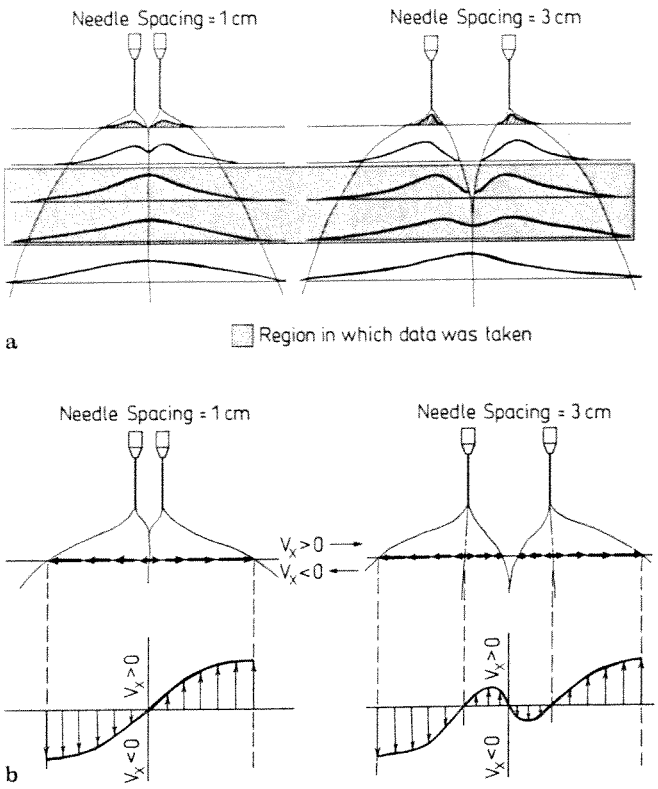

Fig. 5a and b. The relative development of the mean velocity profiles; **a** axial mean velocity profiles with respect to axial position; **b** vector representation of lateral mean velocity profiles

increasing the axial distance from the needles' tips and decreasing the needle spacing both act to enhance droplet mixing and, hence, serve to increase the spatial uniformity of the combined spray. Further evidence for droplet mixing can be found by examining the velocity component–diameter correlations within the mixing region, which is the subject of another paper (Dunn and Snarski 1991).

The effect that the applied voltage had on the mean velocity component profiles also is shown clearly in Figs. 3 and 4. Here, an increase in voltage caused an increase in both the axial and lateral mean velocity components for both needle separations at all points within the spray. The increase in the axial mean velocity components was the result of a greater initial momentum imparted to the droplets because of the increased electric field (hence, electrostatic force) at the needles' tips that occurred with increasing voltage. This trend was only accentuated by the decrease in droplet mass that occurred with increasing voltage (to be presented later). The increase in lateral mean velocity components was a result of the increased electrostatic repulsion between droplets, which was a consequence of the increase in droplet specific charge with increasing voltage.

This increase in lateral mean velocity component also lead to a broadening of the spray. This is not immediately obvious in the previous figures because of the similar horizontal range used in them. It can be seen by noting the change in profile slope at the spray boundary with increasing

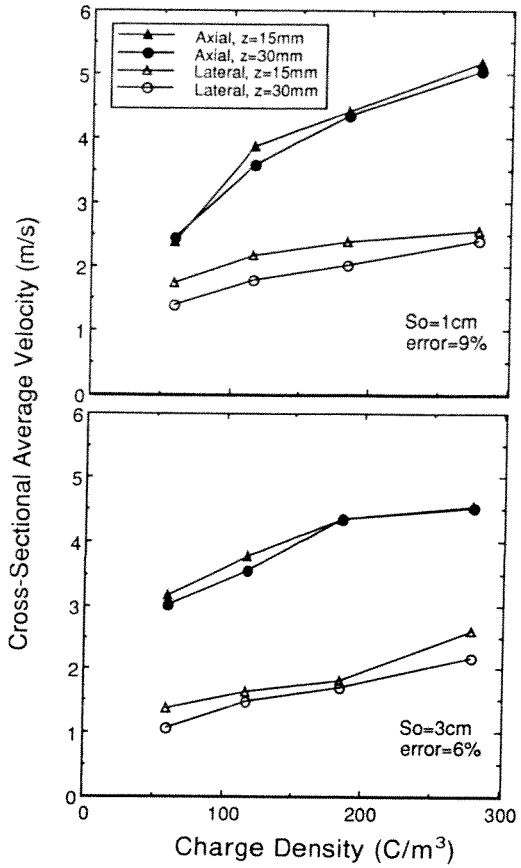

Fig. 6. Cross-sectional average velocities as a function of charge density for 1 and 3 cm needle spacings and 15 and 30 mm axial distances

voltage that is exhibited in those figures. Here, an increase in applied voltage causes a departure from the trend of approaching an asymptotic value of mean velocity component at the farthest lateral measurement position.

The relative magnitudes between the axial and lateral velocity components at any resultant charge density and the effect of charge density on each can be seen in Fig. 6, in which the cross sectional average (csa) value for each mean velocity component profile is plotted as a function of charge density. For the 1 cm needle separation, the csa axial velocity components are approximately twice the magnitude of the csa lateral velocity components at all charge densities. In addition, the csa axial velocity components exhibit a much greater sensitivity to changes in charge density than the csa lateral velocity components, as evidenced by the greater slope. For the 3 cm case, the csa axial velocity components are also all approximately twice the magnitude of the csa lateral velocity components. The change in csa velocity component with increasing charge density is approximately the same for both the csa axial and lateral velocity components. These results verify that a "narrow plume approximation", such as that used by True (1980), in which it is assumed that the lateral velocity component is negligible with respect to the axial velocity component, is not valid for sprays of this nature.

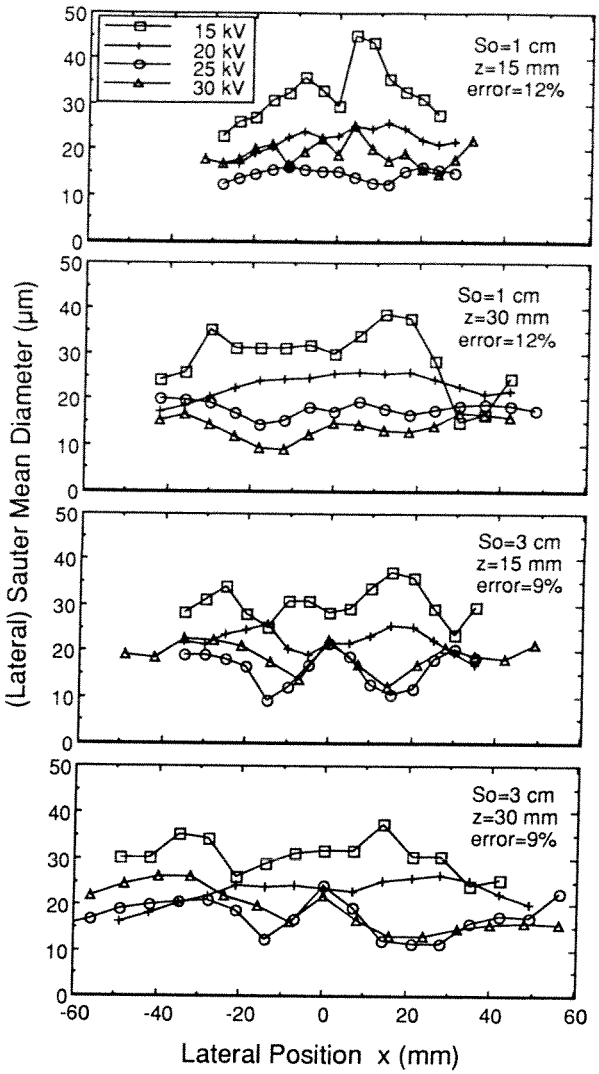

Fig. 7. Droplet lateral Sauter mean diameter profiles for 1 and 3 cm needle spacing and 15 and 30 mm axial distances

4.2 Droplet sauter mean diameters

The Sauter mean diameter profiles across the lateral span of the interacting sprays for both needle spacings are presented in Fig. 7. Each of these diameters is the mean value of the Sauter mean diameter distribution at that measurement point. The total experimental error for the mean diameter that resulted from uncertainties in the PDPA velocity measurement, mass flow rate, probe volume position and needle separation distance were 12% and 9% for 1 cm and 3 cm needle spacings, respectively.

The mean diameter results acquired at a particular position during both the axial and lateral velocity measurements, i.e., with either laser beam orientation, agreed within their margin of experimental error for all cases except one. A typical comparison between the mean diameter data obtained at both laser orientations is shown in Fig. 8. Here, agreement to within a maximum disparity of 9% is shown

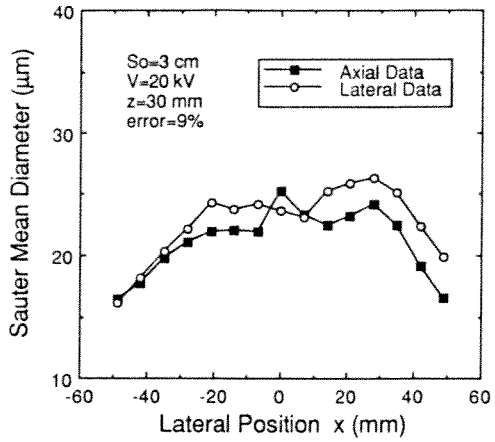

Fig. 8. Comparison between typical axial and lateral Sauter mean diameter profiles

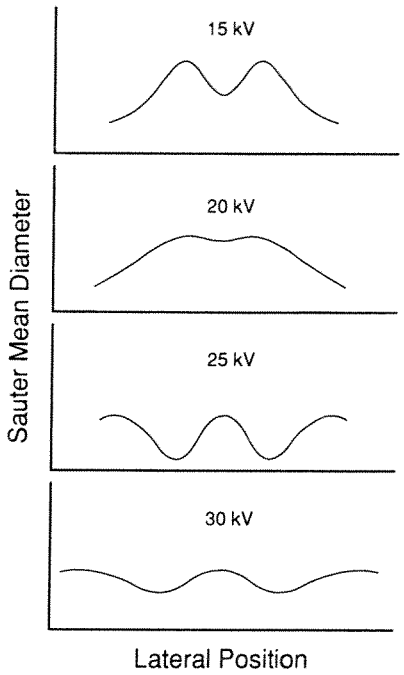

Fig. 9. The typical evolution with increasing voltage of the droplet diameter distribution across the spray

between the mean diameter data acquired during both the axial and lateral velocity measurements at 20 kV and a 3 cm needle spacing. The only exception to such agreement was that case obtained for a 1 cm needle spacing at 15 kV. This was the result of an instability that occurred in the sprays at 15 kV between the times at which the two sets of data were acquired.

The Sauter mean diameter distribution across the lateral span of the sprays was found to be strongly sensitive to the magnitude of the applied voltage, while at the same time, only moderately sensitive to needle spacing and axial position. The evolution of the Sauter mean diameter distribution across the lateral span of the sprays with increasing voltage, as shown in Fig. 7, is illustrated qualitatively in Fig. 9. At

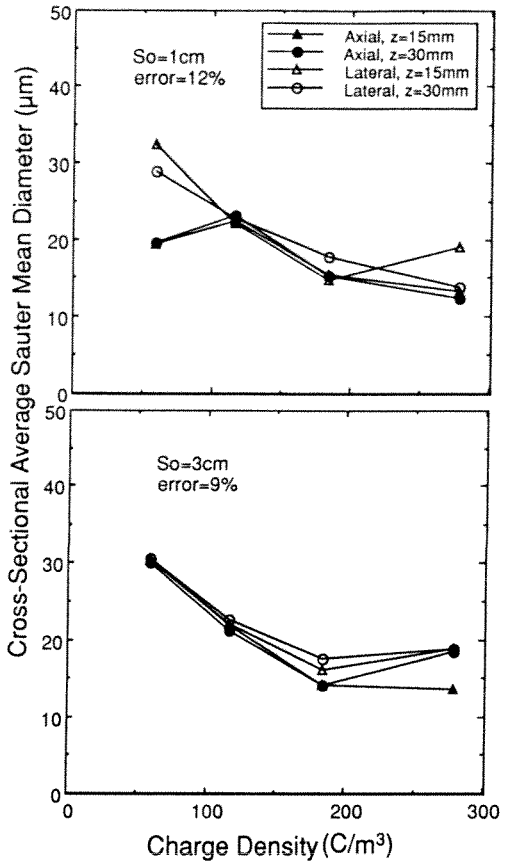

Fig. 10. Cross-sectional average Sauter mean diameters as a function of charge density for 1 and 3 cm needle spacings and 15 and 30 mm axial distances

15 kV, the general profile shape was found to contain two local maxima located at lateral positions along the two needles' centerline axes. An increase in axial distance from the needles' tips or a decrease in needle spacing generally served to decrease the magnitudes of these maxima. At 20 kV, the magnitudes of the two maxima were significantly decreased, resulting in relatively smooth profiles. Again, an increase in axial distance or a decrease in needle separation reduced the magnitudes of the two maxima slightly further. At 25 kV, the profiles typically exhibit three local maxima, one at the centerline and two near either edge of the sprays. An increase in axial position for this case did little more than broaden the profile, while the decrease in needle spacing tended to reduce the magnitudes of the local maxima. The 30 kV profiles were similar to the 25 kV profiles, except the magnitudes of the maxima were attenuated slightly further.

An increase in applied voltage, as shown in Fig. 7, produced a decrease in Sauter mean diameter across the majority of the spray width. This trend of decreasing diameter with increasing voltage was expected, as noted by previous investigators, e.g., Huebner (1969). This can be examined more clearly in Fig. 10, in which the cross-sectional average (csa) value for each Sauter mean diameter profile is plotted as a function of charge density. The two axial data points at

15 kV are not within the margin of experimental error, as mentioned previously. As can be seen, there is, in general, a net decrease in the csa Sauter mean diameter across the range of applied voltages. Although it is possible to speculate from the information contained in Fig. 10 that the csa droplet diameters are asymptotically approaching a contant value at a charge density level of 184 C/m^3, several cases show an increase in diameter at 278 C/m^3. The reason for these increases is not apparent. Figure 10 also illustrates that the csa diameter was not sensitive to needle spacing because the corresponding csa values for most of the charge densities are the same within the margin of experimental error. In addition, as indicated by the data in these figures, no net decrease in csa droplet diameter occurred between the first and second axial positions, implying that any possible droplet evaporation did not affect the results in this region.

Further examination of these data suggest two separate development patterns of the combined spray that are dependent upon the magnitude of the applied voltage and, therefore, charge density. At the lower applied voltages (15 and 20 kV), the profile containing two local maxima evolve toward a profile containing only one. This evolution occurs with an increase in voltage, a decrease in needle spacing or an increase in axial distance from the needles' tips. At the higher voltages (25 and 30 kV), the profiles appear to evolve from one containing three distinct local maxima to a more uniform one in which the magnitudes of the three maxima are reduced. Again, this evolution occurs with either an increase in voltage or a decrease in needle separation. The effect of an increase in axial distance is not as apparent here. For both of these patterns, the parameter changes that bring about this development are in direct agreement with those that brought about the increased development of the velocity profiles.

It is postulated that the difference that exists between the evolutionary patterns of the profiles is the result of a regime transition that occurs somewhere between 20 and 25 kV for this type of experiment. This transition alters the breakup mechanism of the liquid into droplets. Photographic evidence obtained by Snarski (1988) supports this conclusion. At the lower voltages, the predominant breakup mechanism appears to be an advanced stage of the Stable Jet Mode, where the EHD forces acting on the liquid at the needle and in the near field region of the spray generate fine jets of liquid that subsequently form whipping liquid filaments which break up and collapse into droplets, as reported by Snarski (1988). At the higher voltages, the predominant breakup mechanism appears to be the Fine Spray Mode, in which primary droplet generation occurs adjacent to the needle's tip (on a length scale of the order of the needle diameter) rather than in the near field of the spray (on the length scale of the order of the needle's length).

Even so, the presence of this regime transition is not enough to explain the lateral distribution of the droplet average diameters that result. It appears, however, that the beginning of the Fine Spray Mode is characterized by a zone of fine droplets near the axial centerline of a needle's spray, which increases laterally in extent as the applied voltage is increased further. The experimental evidence of Huebner (1969) supports that the relative positions of large and small droplets with respect to the centerline of the spray is not fixed but varies with applied voltage. Only further detailed evidence on the distribution of droplet sizes in a single spray can provide the needed insight into what is occurring between interacting droplet sprays. This is the subject of another paper (Dunn and Snarski 1990).

4.3 Spray photography

Continuous and stroboscopic photographs were used to determine the outer half-width of the spray with respect to the centerline axis of its needle. This was done for each of the two axial positions, two needle spacings and four applied voltages examined in order to possibly quantify the effects of these parameters on the total spray width.

The results of these measurements revealed that between $z = 15$ and 30 mm all the spray half-widths examined increased with axial distance raised to a constant power. The value of this power equalled 0.95, with a standard deviation of 0.13, and was independent of needle spacing and applied voltage. A similar power law behavior is exhibited in the spread of a single-phase circular laminar jet (Schlichting 1979), in which the value of the power is unity.

This relationship between spray half-width and axial distance which is independent of needle spacing and applied voltage suggested that parameters which vary with axial distance, such as the axial velocity component, could be expressed in a self-similar manner. This was ascertained plotting the nondimensional axial mean velocity component, i.e., the axial velocity component divided by its axial velocity component directly below the axial centerline of the needle, as a function of the nondimensional spray half-width, i.e., the lateral distance from the axial centerline divided by the axial distance. This is done for each applied voltage case in Fig. 11, in which the nondimensional axial mean velocity component is plotted versus the nondimensional lateral distance for the two needle spacing and two axial distances examined.

As shown, the nondimensional axial mean velocity component decreases with increasing nondimensional lateral distance independent of needle spacing and axial distance. The shape of this profile is Gaussian in form, which is similar to the axial velocity component profile of a single-phase circular laminar jet (Schlichting 1979). For an applied voltage of 15 kV, the data for the four cases examined agree with each other to within approximately 15% at any nondimensional lateral distance. Better agreement is obtained with increasing voltage, where, at 30 kV, there is agreement to within approximately 6%. This trend is a further indication of the spatial uniformity that occurs in such sprays as they enter the Fine Spray Mode.

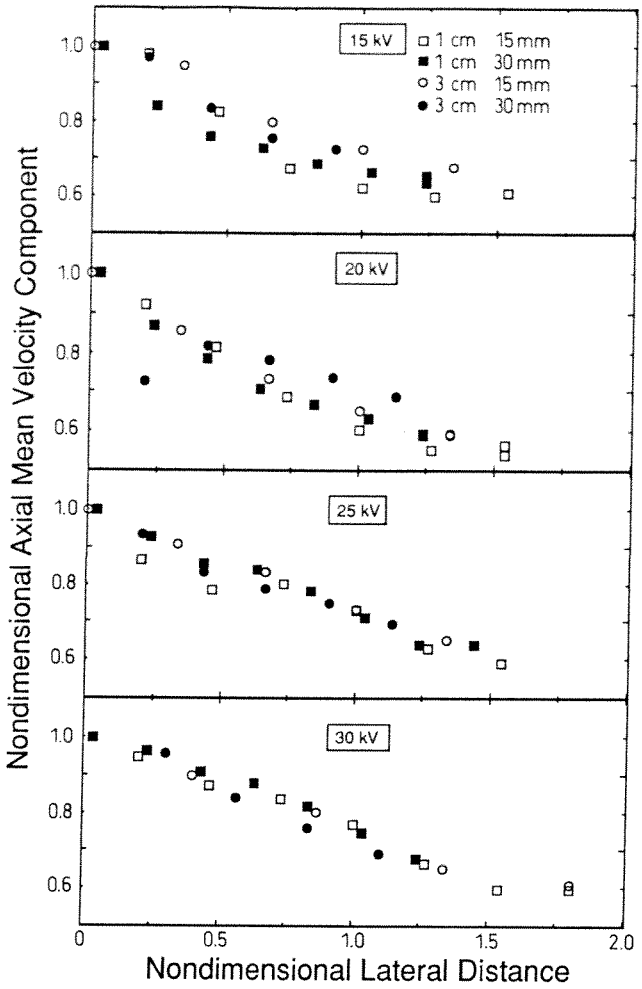

Fig. 11. Nondimensional velocity as a function of nondimensional lateral position for the four applied voltages

Examination of these figures also reveals a slight dependence in profile shape on applied voltage. The magnitude of the nondimensional axial mean velocity component at a fixed nondimensional lateral distance increases somewhat with increasing applied voltage. This is exhibited most noticeably at a value of the nondimensional lateral distance equal to approximately 0.5. The maximum difference obtained between the 15 kV and 30 kV cases is approx. 15%. This suggests a further refinement in the nondimensionalization of the axial mean velocity component, which is not considered herein.

5 Conclusions

By examining the droplet field that results from the interaction between two adjacent and parallel electrohydrodynamically generated droplet sprays, the effects of applied voltage, therefore, spray charge density, and needle separation on the combined spray were deduced. Either decreasing the needle separation or increasing the applied voltage enhanced the mixing between the two needles' droplet sprays and, hence, increased the axial development and spatial uniformity of the combined spray. This, in essence, caused the combined spray to approach one fully developed spray.

Several more specific characteristics of the droplet sprays also were deduced. An increase in the applied voltage produced an increase in both the droplet axial and lateral velocity components. This resulted from the increased electric field intensity and the greater specific charge of the droplets, hence spray charge density, that occurred with increasing voltage. When averaged over the spray cross-section, these axial and lateral velocity component increases were found to be of the same order for the 3 cm needle separation, but were greater for the axial velocity components for the 1 cm needle separation. For all cases examined, the cross-sectional average axial velocity components were approximately twice the magnitude of the cross-sectional average lateral velocity components.

The increase in the applied voltage also yielded, in general, a decrease in the droplet Sauter mean diameter with increasing voltage across a majority of the spray width. For several cases, however, a slight increase in the cross-sectional average Sauter mean diameter occurred between 25 and 30 kV. The cross-sectional average diameter was not sensitive to needle spacing. In addition, the distribution of droplet diameters in the combined spray was found to depend upon the applied voltage. Needle spacing did not affect the distribution of droplet sizes in the spray, but only the relative axial development of the spray.

The lateral spread of the spray also could be characterized quantitatively. The spray half-width was related to axial distance. This revealed that the axial mean velocity component was self-similar with respect to lateral position when expressed in the nondimensional manner presented herein.

In conclusion, these results collectively support that conventional EHD techniques using multiple needles in parallel could be used to effectively atomize liquids at increased flow rates. By appropriately varying the applied voltage, therefore, spray charge density, and the needle separation distance, enhanced mixing can be achieved, thereby creating a spatially uniform, liquid droplet spray.

Acknowledgements

This work was performed under MIPR No. FY76168800343 between the University of Chicago and the Department of Defense and under Contract No. 62622401 between Argonne National Laboratory and the University of Notre Dame. We gratefully acknowledge our technical contacts within the Engineering Physics Division of Argonne National Laboratory (Dr. V. J. Novick, program coordinator, and Dr. E. D. Doss, program manager). The experiments reported herein were part of the M. S. thesis work of S. R. Snarski conducted in the Particle Dynamics Laboratory in the Department of Aerospace and Mechanical Engineering at the University of Notre Dame.

References

Bachalo, W. D.; Houser, M. J. 1984: Phase Doppler spray analyzer for simultaneous measurements of drop size and velocity distributions. Opt. Eng. 23, 583–590

Bailey, A. G. 1974: Energy minimization and charge-to-mass relationships of electrohydrodynamic sprayed liquid droplets. Phys. Fluids 17, 852–853

Bailey, A. G. 1988: Electrostatic spraying of liquids. New York: John Wiley

Clift, R.; Grace, J. R.; Weber, M. E. 1978: Bubbles, drops, and particles. New York: Academic Press

Dunn, P. F.; Snarski, S. R. 1991: Droplet diameter, flux and total current measurements in an electrohydrodynamic spray. Fifth International Conference on Liquid Atomization and Spray Systems, National Institute of Standards and Technology, Gaithersburg, Maryland

Dunn, P. F.; Snarski, S. R. 1991: Velocity component and diameter distribution characteristics of droplets within two interacting electrohydrodynamic sprays. Phys. Fluids A 3, 492–494

Hendricks, C. D. Jr. 1962: Charged droplet experiments. J. Colloid Science 17, 249–259

Hidy, G. M. 1984: Aerosols: an industrial and environmental science. New York: Academic Press

Hogan, J. J.; Hendricks, C. D. 1965: Investigation of the charge-to-mass ratio of electrically sprayed liquid particles. AIAA J. 3, 296–301

Huebner, A. L. 1969: Disintegration of charged liquid jets. J. Fluid Mech. 38, 679–688

Jones, A. R.; Thong, K. C. 1971: The production of charged monodisperse fuel droplets by electrical dispersion. J. Phys. D: Appl. Phys. 4, 1159–1166

Kelly, A. J. 1976: Electrostatic metallic spray theory. J. Appl. Phys. 47, 5264–5271

Kelly, A. J. 1978: Electrostatic-spray theory. J. Appl. Phys. 49, 2621–2628

Kelly, A. J. 1984: Low charge density electrostatic atomization. IEEE Trans. Ind. Appl. IA-20, 267–273

Krohn, V. E. 1974: Electrohydrodynamic capillary source of ions and charged droplets. J. Appl. Phys. 45, 1144–1146

Lue, K-M; Kelly, A. J. 1987: Quadrupole mass spectrometer measurements of electrostatic sprays. Conference Proceedings of Electrostatics '87, The Institute of Applied Physics, Static Electrification Group, St. Catherine's College, Oxford, England

O'Hern, T. J.; Rader, D. J.; Ceman, D. L. 1989: Droplet sizing calibration of the phase Doppler particle analyzer. 1989 Annual Meeting of the American Association for Aerosol Research, Reno, NV

Ogata, S.; Hatae, T.; Shoguchi, K.; Shinohara, H. 1978: The dimensionless correlation of mean particle diameter in electrostatic atomization. Int. Chem. Eng. 18, 488–493

Pfeifer, R. J.; Hendricks, C. D. 1967: Charge to mass relationships for electrohydrodynamically sprayed liquid droplets. Phys. Fluids 10, 2149–2154

Schlichting, H. 1979: Boundary-layer theory. New York: McGraw-Hill

Snarski, S. R. 1988: The interaction of electrohydrodynamically generated liquid droplets. Masters Thesis, University of Notre Dame, Notre Dame, IN

True, M. A. 1980: Modelling of electrostatic spray plumes. Conference Record, Industry Applications Society IEEE-IAAS-1980, 993–997

Received December 10, 1990

Technical notes

Dual-beam-sweep laser speckle velocimetry

M. Kawahashi and **K. Hosoi**

Faculty of Engineering, Saitama University, Urawa, Saitama, 338, Japan

1 Introduction

Speckle velocimetry is a well-known technique to measure the simultaneous distributions of the velocity in a fluid flow. The fluid seeded with small particles is illuminated by a thin sheet of pulsed laser light with a short-time interval between pulses. Speckle patterns (or images of particles) produced by the moving particle field within the light sheet are recorded as double- or a multi-exposures.

The recording of speckle patterns on photographic film is limited by the amount of light scattered from the particles. A high-power, double-pulsed laser with very short pulse duration is usually applied for the illumination. A continuous wave laser can also be used by combining it with a beam chopper. The pulsed laser beam is normally expanded by means of a lens system to form a plane fan-like sheet in the flow.

In a previous paper (Kawahashi and Hosoi, 1989) we described a new technique of illumination by periodical beam sweep with CW laser light. This type of illumination provides not only a stroboscopic effect like pulsed-light illumination, it is also more intense than a normal light sheet. However, when this technique is applied to high speed flow, a high speed beam scanner is needed. The increased sweep velocity then decreases the amount of light scattered from tracer particles.

In order to improve these shortcomings of the technique, an illumination by dual-beam-sweeps (DBS-LSV) is proposed in this note.